Version of Record: https://www.sciencedirect.com/science/article/pii/S1385894721055339
Manuscript_dbbed054bd2bfa4abcef103fa7c4db7d

Temperature-dependent Dynamic Fouling on Superhydrophobic and Slippery Nonwetting Copper Surfaces

S.M.A. Mousavi and R. Pitchumani[1]

Advanced Materials and Technologies Laboratory

Department of Mechanical Engineering

Virginia Tech

Blacksburg, Virginia, VA 24061-0238

ABSTRACT

Bioinspired, superhydrophobic and slippery liquid infused surfaces that offer nonwetting characteristics have been explored in recent years for fouling mitigation. However, most of the studies are in the context of biofouling or under static immersion at ambient temperature conditions that are not reflective of the dynamic flow environment in practice. This article presents, for the first time, a systematic study of dynamic fouling of superhydrophobic (SHS) and slippery lubricant-infused surfaces (LIS) over a range of flow and temperature conditions. Copper metallic surfaces were textured via electrodeposition or etching and further functionalized to achieve SHS and, additionally, infiltrated with a lubricant to fabricate LIS. The nonwetting surfaces were studied for their fouling behavior in a rotating Couette flow of a supersaturated calcium sulfate solution at different rotational speed and temperature. Fouling mineral mass accumulation on the different surfaces was measured as a function of time over a period of days using inductively coupled plasma mass spectroscopy and the fouled surfaces were investigated using scanning

[1] Corresponding Author; pitchu@vt.edu, +1 703 538 3772

electron microscopy. Both SHS and LIS showed superior anti-scaling performance at all ranges of variables. An analytical Hill-Langmuir model is presented, for the first time, to describe the time evolution of scaling within 20% accuracy over the range of parameters studied. The study is the first to juxtapose two surface texturing methods, electrodeposition and etching, and two nonwetting surface types, SHS and LIS, subject to a common suite of experiments to elucidate fundamental understanding of mineral fouling on nonwetting surfaces.

KEYWORDS: multiscale texturing; superhydrophobicity; lubricant-infused surface; anti-scaling; Hill-Langmuir model

1. INTRODUCTION

Fouling occurs on surfaces in two major ways: biological fouling and crystallization fouling; the latter—also called *scaling*—due to crystallization of salt ions onto a surface is the focus of this article. An excessive scaling of heat transfer surfaces by the soluble salts in a process fluid imposes performance degradation and maintenance cost. Phosphates, sulfates, and carbonates of calcium are among the salts that usually cause scaling, of which calcium sulfate is one of the most commonly reported in various industries such as seawater desalination[1], geothermal power plants working with brine[2], nanofiltration devices[3], heat exchangers[4], and condensers[5]. Consequently, there has been a lot of attention to understanding the underlying mechanism of mineral crystallization[6,7], in general, and calcium sulfate scaling, in particular[8–10].

Heterogeneous nucleation is a surface phenomenon that depends on several parameters including the saturation level of solution and surface properties like roughness and surface energy. Moreover, adhesion of the nucleated crystals to the surface is a function of surface properties as

well as forces exerted from the solution to the crystal. Efforts for mitigating scaling fall into two general categories [11]. In one approach, the chemistry of the process/working fluid in contact with the metallic surface is modified in a way to deter the onset of nucleation, increase the solubility of the salt ions or dissolve the scaled salts by flowing harsh acidic fluids[12]. These methods, however, suffer from the adverse effect of the added chemicals on the fluid thermophysical properties, deterioration of the metallic surfaces themselves as well as environmental concerns of the additives [13]. The second approach of modifying surfaces to deter crystallization has attracted more attention from the scientific community in recent years[14–18]. Using this approach, studies have been reported on the scaling of calcium on different silicon surfaces with different surface energies, which suggest that lowering the surface energy on surfaces reduces scaling rate[19]. Moreover, there have been several studies on the effect of surface roughness and its effect on the extent of scaling[20–23]. Most of the literature suggests higher roughness to cause a higher scaling rate[24]; however, few studies show the reverse effect[25,26]. The contradictory observations in the literature may be attributed to the size of the surface roughness, although studies to isolate the effect of roughness are not available in the literature.

Among surface modification techniques, there has been an increasing number of studies on hydrophobic and superhydrophobic surfaces (SHS) against scaling, as well as slippery lubricant-infused surfaces (LIS) for their promising nonwetting properties. According to Jiang et al.[27], a superhydrophobic CuO nano-wire layer was formed on a Cu foil for use in the anti-scaling of $CaCO_2$. Anodization was used to create the CuO nanowire layer on the copper surface, which was the initial step. The water CA on the CuO nanowire increased dramatically after being coated with FAS-17, going from hydrophilic 4.5° to superhydrophobic 154°. Furthermore, the scaling weight

of attached $CaCO_3$ fell from 0.6322 to 0.1607 mg cm^{-2}. The test was done for 2 h at static condition in mixed solution of $CaCl_2$ and $NaHCO_3$ at 90 °C.

Qian et al.[28] developed a superhydrophobic polymer coating based on poly(phenylene sulfide)/polytetrafluoroethylene (PPS/PTFE) composites on steel as the substrate. The deposition rate of scaling on the superhydrophobic PPS/PTFE coating was 38.6% of that on the hydrophobic epoxy-silicone resin coating. The scaling experiment was done by static immersion in calcium containing solution at 60 °C. Charpentier et al.[29] used liquid-infused porous surfaces to investigate their potential to suppress $CaCO_3$ scale formation. They began by covering stainless steel substrates with microporous polypyrrole (PPy) coatings. Then, lubricant liquids with low surface energy, such as fluorinated lubricant (FC-70) and ionic liquid were infused to create liquid-repellent slippery surfaces. They discovered that PPy surfaces infused with ionic liquid had exceptional antifouling capabilities after 2 h immersion in static bulk jar of calcium carbonate at 50 °C when compared to untreated stainless steel.

Varanasi and colleagues[16] presented lubricant-impregnated nanostructured surfaces to obtain the requisite resistance to mineral scales. Using reactive ion etching, they first created a flat silicon surface with nanograss structures. To reduce its surface energy, they treated it with octadecyltrichlorosilane (OTS). Silicone oil and DC704 have been impregnated further into the OTS-coated nanograss substrate, respectively. In a static test bath of $CaSO_4$ at 40 °C for 80 hours, the silicone oil-impregnated nanostructured silicon surface displayed antiscaling capabilities when compared to the uncoated smooth silicon surface. Similarly, LIS were made by infusing Krytox105 silicon oil into electropolymerized and silanized porous polyaniline, as described by Sousa et al.[30] In short, hierarchically rough polyaniline was electropolymerized onto stainless steel substrates and then further functionalized with low polarizability thiols (1H, 1H, 2H, 2H-

perfluorodecanethiol, PFDT) to create superhydrophobic surfaces. LIS have a better preventive effectiveness against inorganic scales than nonlubricated surfaces. The tests were carried out for in static jar test at room temperature for 16 h.

It is evident from the foregoing discussion that while scaling on SHS and LIS under static conditions is well-studied, there is a conspicuous shortage of studies exploring the response of SHS and LIS to scaling under dynamic flow conditions that are encountered in several applications. Furthermore, there is nearly no theoretical model available for scaling that can be used for designing the surfaces for applications or for understanding the extent of scaling on a target surface.

The goal of the present study is to address the above knowledge gaps by considering scaling of calcium sulfate, the most common contributor to scaling in the industry, on copper, a widely used heat transfer surface in engineering systems. Copper metallic surfaces were textured and further functionalized to achieve SHS and, additionally, infiltrated with a lubricant to fabricate LIS. Surface texturing was achieved using electrodeposition, an additive method, or chemical etching, a material removal method. Systematic parametric experiments were conducted to explore, for the first time, the effects of dynamic flow conditions and temperature on scaling of SHS and LIS fabricated by the two methods. A Hill-Langmuir relationship is developed based on experimental data to model time evolution of scaling on nonwetting surfaces. The study juxtaposes, for the first time, two surface texturing methods, electrodeposition and etching, and two nonwetting surface types, SHS and LIS, subject to a common suite of experiments.

The article is organized as follows: In the next section, section 2, the experimental methods for fabrication of surfaces, dynamic fouling, and surface characterization are presented. Results of the

full set of parametric tests on dynamic fouling and the kinetic model are described in section 3 on Results and Discussion. The principal findings of the study are summarized in section 4.

2. EXPERIMENTAL METHODS

2.1 Materials and reagents

Hydrochloric acid (HCl), analytical-grade copper sulfate ($CuSO_4$, 99+%), sulfuric acid (H_2SO_4), acetone (99.5+%), methanol (99.8+%), and stearic acid ($CH_3(CH_2)16CO_2H$, 97%) were purchased from Fisher Scientific (Pittsburgh, PA, USA) and used as received without any further purification. Hydrogen peroxide solution (H_2O_2) was purchased from Sigma-Aldrich (St. Louis, MO, USA), deionized water of resistivity 14MΩ.cm was purchased from CQ Concepts (Ringwood, IL, USA), silicone oil, Dowsil500™, was purchased from DuPont (Wilmington, DE, USA), and plain multipurpose copper sheet was purchased from McMaster (Elmhurst, ILUSA).

2.2 Fabrication of nonwetting surfaces

Fabrication of superhydrophobic (SHS) and lubricant-infused surfaces (LIS) was carried out by first texturing the surface, functionalizing the textured surface to create SHS, and additionally by infiltrating the porous textures with a lubricant liquid to create LIS. The as-received copper sheet was cut into coupons of 1×5 cm, and the coupons were degreased and cleaned by 5 minutes sonication in acetone, followed by 5 minutes sonication in ethanol, then rinsed with DI water and dried in a nitrogen stream. In the material *removal* method of texturing, the roughness features were carved into the surface via chemical etching in an aqueous solution of 0.02 M hydrochloric acid and 0.05 M hydrogen peroxide. The cleaned and cut coupons were submerged in the etchant solution for 20 minutes. In the *additive* method of texturing, multiscale asperities were grown on top of the copper surface by a three-electrode, two-step electrodeposition process[31],[32] using

an AUTOLAB PGSTAT128N electrochemical station (ECO Chemie, Utrecht, The Netherlands). A platinum mesh was used as the counter electrode and Ag/AgCl served as the reference electrode. De-aerated aqueous solution of 1M $CuSO_4$ and 0.5M H_2SO_4 was used as the electrolyte. The two-step electrodeposition process was initiated by applying –1.1 V for 5 minutes to the copper sample as the working electrode followed by a 10 second electrodeposition at –0.15 V as the second step. The second deposition served to further stabilize the first coating onto the surface.

All the prepared textured surfaces were rinsed in DI-water bath and dried under vacuum at 110 °C overnight. As the next step, the textured surfaces were chemically functionalized via 24 h immersion in 0.02M stearic acid, which provided for reducing the surface energy through chemisorption of the long-chain fatty acids onto the surface. Stearic acid is chosen as an environmentally friendly chemical[33] compared to the other functionalization agents such as silane and perfluorinated compounds that are toxic[16,34,35]. The stearic-acid-functionalized surfaces exhibited a water contact angle over 150 degrees with low surface energy, forming superhydrophobic surfaces. LIS was fabricated by infusing the SHS with lubricant oil. Drops of Dowsil™ silicone oil with 500 cSt viscosity were placed onto the SHS and hanged vertically for twenty minutes to allow for the lubricant to wick into the interasperity spaces and to drain any excess oil.

The SHS and LIS fabrication processes are versatile in their applicability to a variety of metallic materials of complex geometry and size. Copper was chosen as one of the ubiquitously used materials to perform dynamic scaling experiments.

2.3 Dynamic fouling setup

Dynamic fouling was studied using an annular Taylor-Couette flow [36] set up in which a rotating cylindrical drum of radius 10 cm was placed concentric inside an outer stationary cylindrical tank of radius 18 cm, as depicted in Figure 1. The rotation of the inner drum was driven by a motor with a vertical shaft, such that the rotational speed can be set to desired values. The annulus between the inner cylindrical drum and the outer cylindrical tank was filled with supersaturated $CaSO_4$ solution in water. The test coupons were mounted on the outer surface of the inner drum such that they experienced a dynamic shear due to the rotational fluid flow in the annulus. The setup was placed on a hot plate so that the solution can be heated to a desired temperature, measured using a thermometer with a digital readout, immersed in the solution in the annulus. A feedback control loop was used to control the hot plate to achieve a set point temperature of the scaling solution. The open tank configuration follows that used in static scaling studies in the literature[19,37], and provided for maintaining solution supersaturation required for crystallization.

Dynamic fouling experiments were conducted on superhydrophobic and lubricant-infused copper surfaces fabricated by electrodeposition and etching, at three rotation rates of 100, 200 and 400 rpm, and at two different temperatures, 23 °C and 50 °C. In addition, for reference, dynamic fouling studies were also conducted on bare copper coupons at the three rotational speeds and the two temperature values. Based on the reverse solubility curve of calcium sulfate hemihydrate ($CaSO4.\ 0.5\ H_2O_2$) with temperature [38,39], 7.0 g and 5.0 g gypsum were mixed in 1 liter of deionized water to prepare supersaturated solution for test at 23 °C and 50 °C, respectively. The turbulent nature of the test ensures consistent mixture of the calcium in the solution. In each case, to understand the time evolution of scaling, coupons were removed at time durations of 12, 24, 48,

96 and 192 hours from the start of the experiment. Three replicates were analyzed at each parametric combination of surface type, rotation speed, temperature, and time duration for a total of 240 tests in the overall experimental matrix.

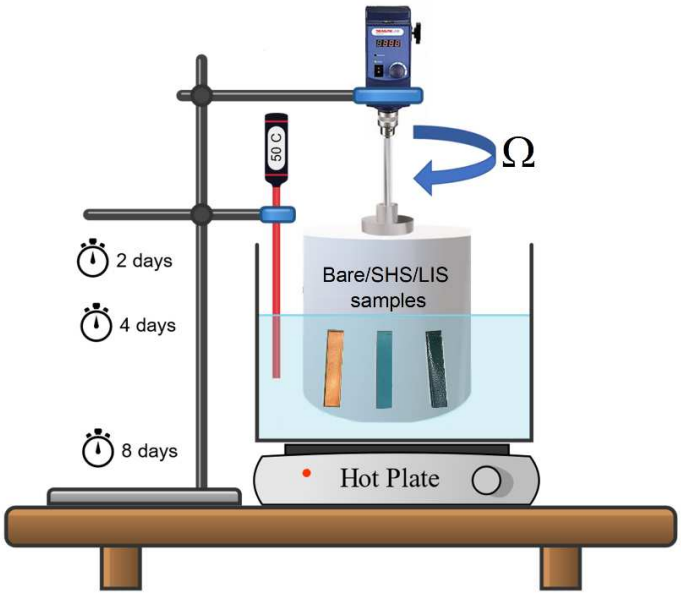

Figure 1: Schematic of the dynamic scaling setup depicting metallic coupons mounted on the outer surface of the inner rotating drum in a stationary cylindrical tank filled with $CaSO_4$ hemihydrate solution.

2.4 Characterization

Samples of the different surface types and fabrication methods were characterized for their surface morphology and wetting characteristics. Surface morphology was revealed via a field-emission scanning electron microscope (SEM) (JEOL 2100, Japan), operating at an acceleration voltage of 20 kV connected to an energy dispersive x-ray analyzer (OXFORD, UK). Optical image of lubricant infused surfaces was obtained via Nikon Eclipse LV100ND Microscope (Nikon Instruments Inc., Japan) equipped with an epifluorescence filter. The apparent contact angle of the surfaces was characterized by a goniometer (ramé-hart model 590, NJ USA) via sessile droplet

method and 10 µl DI-water and at least at five different positions on each sample. The sliding angle was measured via tilting plate method by the same apparatus with 25 µl DI-water.

Weight measurement of the samples before and after the fouling tests is a common way of quantifying the extent mineral deposits in static tests. In a dynamic test, however, since there might be loss of infused liquid, functionalization material, or the base material iteslf from the surface due to shear, erosion or corrosion, an alternative method was used. Following removal of a coupon from the dynamic fouling setup, the sample was dried for 24 hours at room pressure and temperature to remove any moisture. The dried coupon was immersed in 10 ml of 10% nitric acid (HNO_3) for 10 minutes to dissolve the scaled material into the solution. The solution was then diluted and prepared for measurement of calcium concentration using inductively coupled plasma mass spectroscopy (ICP-MS) (Thermo Electron X-Series, Waltham, MA, USA), which had an accuracy of 0.5 $\frac{\mu g}{L}$. The ICP-MS results on the scaling mass were divided by the sample planar surface area to obtain mass gain per unit surface area—termed *fouling density,* m_f''—for a quantitative characterization of fouling.

3. RESULTS AND DISCUSSION

3.1 Surface wettability and morphology

The functionalization step in the fabrication of SHS and LIS coats a layer of stearic acid with low surface energy on the textured surface. In this process copper reduces to Cu(II) oxide and stearic acid chemisorbs onto the surface via $Cu_2O + 2CH_3(CH_{16})COOH \rightarrow 2Cu[CH_3(CH_{16})COO] + H_2O$ pathway [31]. The physics behind fabricating LIS requires preparing the surface such that the lubricant has a greater affinity to the surface compared to the surrounding fluid which is sought to

be repelled from the surface [40]. This was achieved by tuning the surface roughness, solid surface energy through functionalization, and selecting a proper lubricant. Surface wetting properties of the electrodeposited and etched SHS and LIS were measured in terms of deionized water contact angle (CA) and sliding angle (SA). As shown in Figure 2(a), the electrodeposited and etched copper surfaces after 24 h functionalization in stearic acid exhibit contact angle above 155° (orange markers) and very low roll-off angle below 5° (blue markers) which categorize them as superhydrophobic surfaces (SHS) in contrast to bare copper with contact angle of 82° ± 3.4°. Both the electrodeposited and etched lubricant-infused surfaces (LIS) revealed an apparent contact angle of ~92° (orange markers) and a water sliding angle below 5° (blue markers) that attest to the excellent slipperiness characteristic of the surfaces.

The morphology of the copper surface textured by electrodeposition and functionalized with stearic acid is shown in the scanning electron microscope (SEM) image in Figure 2(b). The inset in the figure shows the surface prior to functionalization and reveals that the Cu^{2+} cations were deposited onto the surface in the form of Cu(s)[41] cauliflower-shaped features. The multiscale features covered the surface uniformly with micro and macro size cauliflower asperities exhibiting average diameter as small as 5 µm and as big as 30 µm. After functionalization with stearic acid, the cauliflower asperities were covered with the thin (nanometer thickness) leaflike chemisorbed functionalization agent in final form of dahlia-flowerlike structures (in micron diameter range) as seen in the main image of Figure 2(b). Figure 2(c) shows the microstructure of an etched, functionalized copper surface. The inset micrograph in Figure 2(c) reveals random nano/micro-sized grooves on the as-etched surface before functionalization. The surface morphology of the functionalized etched copper in Figure 2(c) shows the surface to be carpeted with chemisorbed stearic acid that appears as needle-like and sparse pom-pom ball structures in varying sizes up to

about 20 µm in diameter. The hierarchical asperities on the textured surfaces provide a larger surface area compared to the bare smooth surface for chemisorption and growth of the stearic acid structure seen in Figure 2(b) and (c).

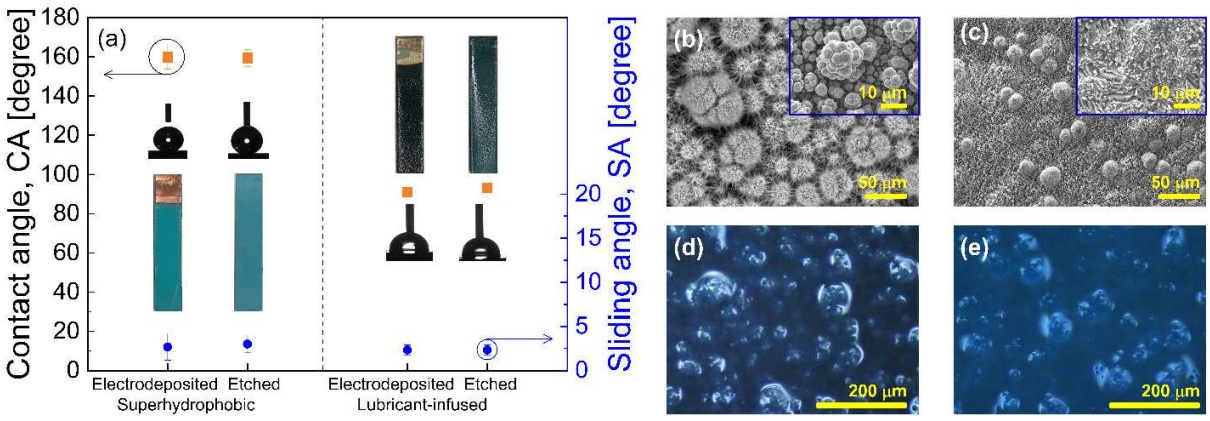

Figure 2: Nonwetting properties and morphology of textured and modified copper surfaces: (a) water contact angle and roll-off/sliding angle of SHS and LIS fabricated via electrodeposition and etching. Inset images are of 5 cm × 1 cm fabricated coupons; SEM images of (b) electrodeposited, functionalized SHS, inset showing unfunctionalized electrodeposited copper surface, and (c) etched, functionalized SHS, inset showing unfunctionalized etched copper surface; Optical images of (d) electrodeposited and (e) etched LIS.

Optical images of electrodeposited and etched LIS are shown in Figure 2(d) and (e), respectively. The underlying dahlia-flowerlike functionalized asperities of electrodeposited LIS appear prominent after the lubricant infusion compared to the pom ball-like structure of the etched LIS. This can be attributed to the differences between the size and sparsity of these structures on the two surfaces.

3.2 Effect of rotation rate on dynamic fouling

The effect of shear due to fluid flow on the extent of scaling on the nonwetting surfaces in comparison to the bare copper surface was studied through a suite of parametric tests that spanned three different rotational speeds and two temperatures. The Reynolds number corresponding to the rotational speeds of 100, 200, and 400 rpm are 49,000, 99,000, and 198,000, respectively, which correspond to the turbulent flow regime. As a point of reference, the Reynolds number for coolant water flow in a typical power plant condenser pipe of 23 mm internal diameter and flow speed of 1.8 m/s–2.5 m/s is in the range 44,000–62,000. The considered range of Reynolds number in the parametric studies elucidate the scaling dynamics for applications of the advanced functional surfaces to high flow rate and/or large pipe flows.

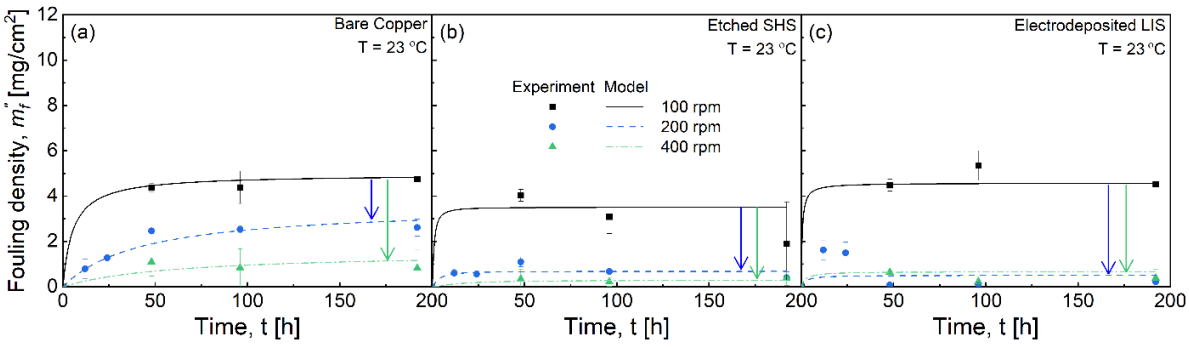

Figure 3: Effect of rotation rate on fouling density evolution with time for (a) bare copper, (b) etched SHS, and (c) electrodeposited LIS, at 23 °C.

The time-evolution of fouling density (m_f'') for the as-received bare copper is shown in Figure 3(a) for different rotation rates at 23 °C. Regardless of the rotational speed, the measured mineral fouling mass density reached a steady state, called the asymptotic fouling mass density, $m_{f\infty}''$, at long duration in the experiments. Figure 3(a) further demonstrates a considerable change in m_f'' and, in turn, $m_{f\infty}''$ with the rotational speed: the highest calcium deposition was recorded at 100

rpm as $m''_{f\infty}$ = 5 mg/cm^2, which decreased with increase in the rotational speed. Mineral deposition on the surface results from an equilibrium between the adhesion forces that draw the minerals to the surface and the shear forces due to the flow that tend to remove the mineral deposits from the surface. The observed decrease in $m''_{f\infty}$ with rotational speed correlates with the increased shear stress with increasing rotation rate (Reynolds number) that shifts the equilibrium towards lower fouling density.

Similar parametric tests were performed for SHS and LIS fabricated via electrodeposition and etching. For brevity, one set of results for etched SHS and electrodeposited LIS is illustrated from the full parametric test experimental matrix, in Figures 3(b) and 3(c), respectively. The physical trends with respect to time and rotation rate follow those for the bare surface. Of note is the reduction in the asymptotic fouling density for SHS and LIS compared to the bare surface, which is particularly greater at the higher rotational rates. The result points to the fact that for a given rotation speed, since the shear forces are identical across surface types, the nucleation of fouling and adhesion of minerals on the nonwetting SHS and LIS is substantially reduced compared to the bare surface, which leads to beneficial reduction in $m''_{f\infty}$. The lines through the experimental data markers in Figure 3 are obtained from the Hill-Langmuir model discussed later in this section.

3.3 Effect of temperature on dynamic fouling

Calcium sulfate in all its hydration forms, hemihydrate and dihydrate, exhibits an inverse solubility variation with temperature which, in turn, manifests in the differing fouling behavior with temperature. In practical applications, process fluids flow at different temperatures, and it is of interest to understand the effect of temperature on the extent of scaling. To this end, dynamic fouling studies were conducted at a low temperature of 23 ℃, and a high temperature of 50 ℃.

The amount of calcium sulfate hemihydrate dissolved into DI water was chosen based on the solubility curve and to maintain the same supersaturation level at the two temperatures.

Figure 4(a) depicts the effect of temperature on the extent of scale mass gain on the as-received bare copper coupons versus time, for an intermediate rotational speed of 200 rpm. The fouling density is seen to be higher at 50 °C due to the higher rate of nucleation and the higher rate of crystallization growth. Based on heterogeneous nucleation theory[42], nucleation rate varies as the temperature to the power of 3 while crystal growth rate varies linearly with temperature, both contributing to the higher fouling density with increasing temperature. The aggressive fouling combined with the fact that the solubility of calcium sulfate hemihydrate at 50 °C is about 40% lower than that at 23 °C, the scaling is seen to reach an asymptotic value at the lower temperature, but not at the higher temperature, in the duration of the experiments.

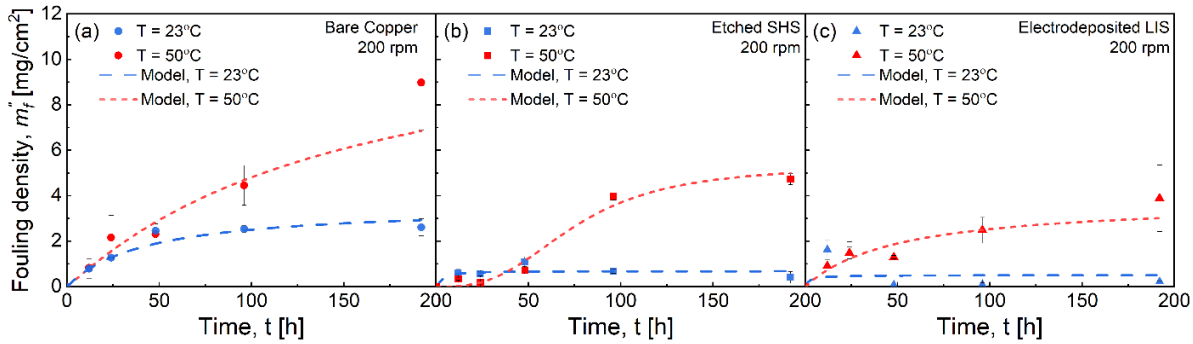

Figure 4: Effect of temperature on fouling density evolution with time for (a) bare copper, (b) etched SHS, and (c) electrodeposited LIS, at 200 rpm.

Figures 4(b) and 4(c) present the effect of temperature on the time-evolution of dynamic scaling for etched SHS and electrodeposited LIS, respectively, at a rotational speed of 200 rpm. Both plots show the enhanced scaling at the higher temperature, following the trend in Figure 4(a); however, at each temperature, the fouling density is lower for the nonwetting surfaces in

comparison to the corresponding fouling density of the bare surface, due to the lower surface energy of SHS and LIS which weakens the adhesion and growth of the mineral deposits on the surface. The reduced strength of adhesion and driving force for deposition relative to the removal of the deposits by shear, also manifests in attaining the asymptotic fouling density at an earlier time for the nonwetting surfaces at 50 °C (Figures 4(b) and 4(c)), compared to the bare surface at the same temperature (Figure 4(a)). As in Figure 3, the lines through the experimental data markers in Figure 4(a)–(c) are obtained from the Hill-Langmuir model discussed later in this section. Overall, even though increase in temperature intensifies the rate of scale nucleation and the rate of scale crystal growth, the nonwetting surfaces fabricated in this study are seen to inhibit scaling substantially. Moreover, SHS and LIS in the study also withstood the higher temperature condition of the tests without degradation.

3.4 Effect of surface type on dynamic fouling

While Figures 3 and 4 showed the effects of rotation rate and temperature considering selected nonwetting surfaces, it is instructive to examine the effects of fabrication and surface type on the resulting scaling of the surface under dynamic conditions. To this end, Figure 5 juxtaposes the different surfaces and fabrication methods with regard to the fouling density at three different times, for the case of 200 rpm at 23 °C. The results reveal that in comparison to bare copper, all the nonwetting surfaces are characterized by a remarkably reduced fouling density. Among the nonwetting surfaces, of the two fabrication methods, electrodeposition yields greater scaling mitigation compared to etching, owing to the rougher multiscale asperity morphology and greater nonwettability of the surface. In the case of electrodeposited LIS, the deeper asperity structures allow for greater lubricant infusion and retention compared to the etched LIS, thereby increasing

the resistance to scaling. With respect to the asymptotic fouling density (192 h), however, there is no distinct difference among the two fabrication methods or surface types, considering the error bars. Furthermore, the values of the asymptotic fouling density for the nonwetting surfaces are all less than about 0.75 mg.cm^{-2} that represent negligible fouling to be of any practical interest. They all lead to over 75% reduction in fouling density compared to bare copper. Nevertheless, based on the mean values, it may be inferred from Fig. 5 that the fabrication method (electrodeposition) has a greater influence on the anti-scaling characteristic.

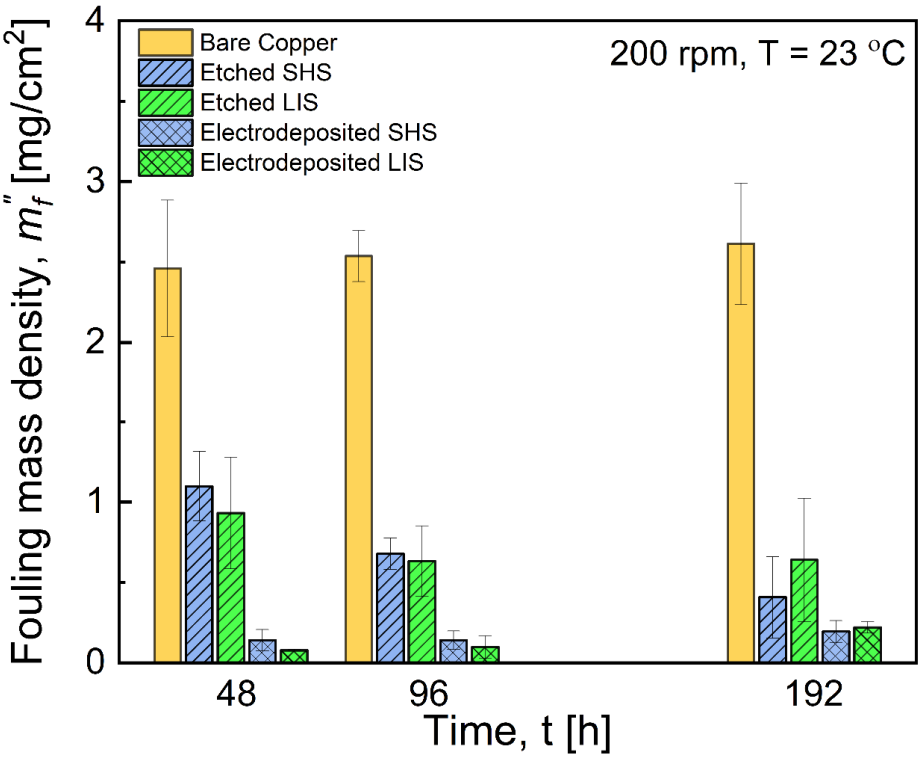

Figure 5: Variation of fouling density with time for the different surface types, at 200 rpm and 23 °C.

The effect of surface type on dynamic scaling was further investigated qualitatively via surface images after scaling for 48 h in the dynamic fouling experiments. Figure 6 shows SEM and optical

images of bare, etched superhydrophobic and electrodeposited lubricant-infused copper surfaces after the dynamic scaling test at 200 rpm and 23 °C. The SEM image in Figure 6(a) shows extensive areas of scaling on the bare copper surface, while the SEM and optical images of SHS and LIS in Figures 6(b) and 6(c), respectively, reveal the sparsity of scaling deposits on the nonwetting surfaces. Quantitatively, over 60% of the surface area of the bare copper is covered with calcium sulfate deposits, while at the similar test condition the SEM image of etched superhydrophobic surface in Figure 6(b) shows ~4% surface area covered with foulant. In the optical image of the electrodeposited LIS, Figure 6(c), very small surface area (less than 4%) is seen to be covered with foulant. The extent of surface coverage is in agreement with the fouling density measurements from the ICP-MS reported in Figures 3–5.

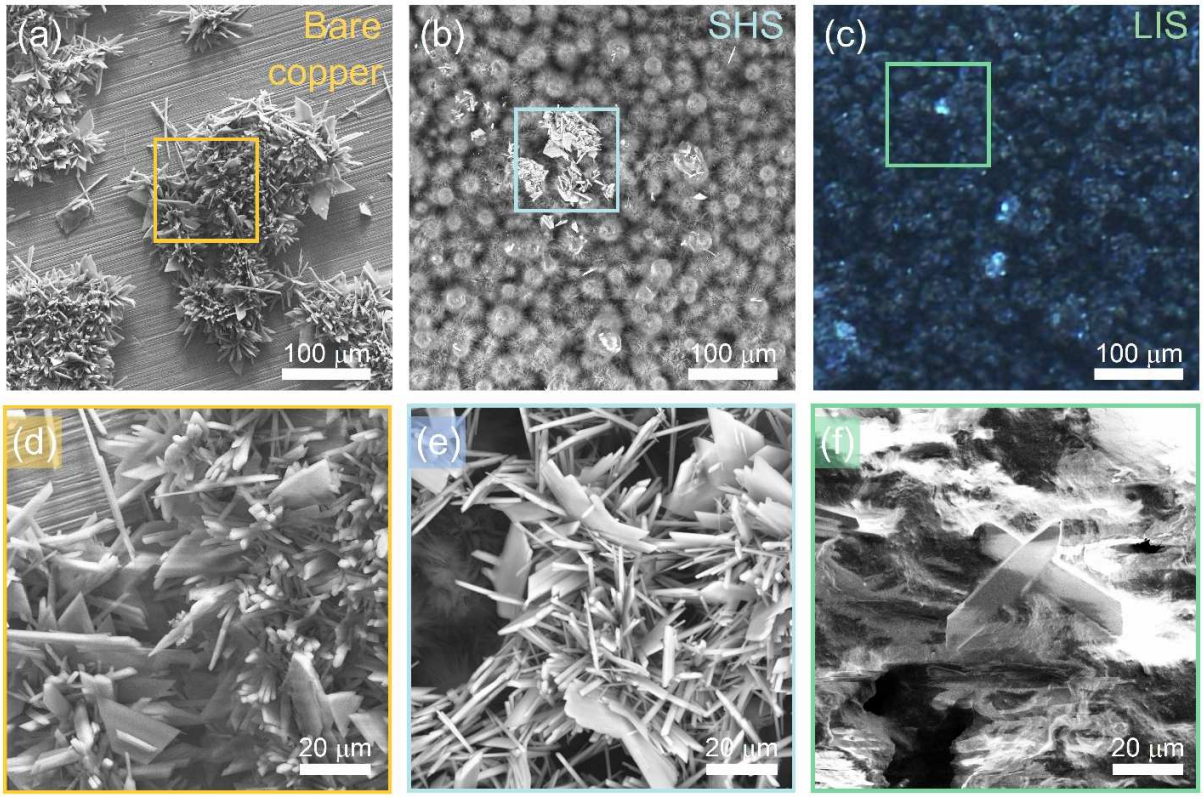

Figure 6: SEM and optical images of copper surfaces after 48 h dynamic scaling experiment at 200 rpm and 23 °C: SEM images of (a, d) bare copper, (b, e) etched superhydrophobic copper, (f)

electrodeposited lubricant infused copper, and (c) optical image of electrodeposited lubricant infused copper surface taken with fluorescent filter.

The higher magnification SEM images in Figure 6(d-f) reveal more of the morphology and structure of calcium scaling on the bare, superhydrophobic and lubricant infused copper surfaces, respectively. The crystalline structure of the deposits is evident in all the micrographs that result from ion packing inside the crystal lattice such that attractive forces are maximized and repulsive forces are minimized[43]. Figure 6(d,e) show rhombohedral crystal units grown and accumulated on the stepped and kinked faces (S and K faces) forming two-dimensional leaf-like flakes on bare and superhydrophobic copper surfaces, along with accumulation on flat face (F face) to form needle-like gypsum crystal structure with rhombohedral and mostly hexagonal plane. The leaf-like flakes are consistent with the maple-leaf-like calcite crystals reported on CuO nanowire films in the literature[27]. The relatively scant calcium sulfate deposits on LIS in Figure 6(f) are seen to be in form of the needlelike crystals. Overall, Figure 6 shows the anti-scaling effect of the nonwetting surfaces and qualitatively supports the quantitative findings in Figures 3–5.

3.5 Modeling

Modeling of fouling on conventional surfaces has been studied in prior literature[44],[45], as reviewed in treatises such as Webb and Li[46]. In general, fouling models for conventional surfaces fall into one of four categories: linear, falling-rate, power law, and asymptotic or sigmoidal. The wide range of models reflects the large uncertainty inherent in the fouling process itself[47,48]. There is no prior modeling effort reported to describe scaling on nonwetting surfaces, and the present study seeks to contribute the first model describing scaling on SHS and LIS as well

as smooth surfaces, in a generalized manner. To this end, we adopt a model that is a good representation of the experimental data, has a closed-form mathematical expression, and has a physical correlation to the phenomenon being modeled.

The measured experimental data on time evolution of fouling density in this study (Figures 3 and 4) show not only sigmoidal trends but also a power law variation. Such data can be well-described by the Hill-Langmuir equation[49,50] that is widely used in biochemistry for explaining different phenomena such as binding of ligands to macromolecules[51].

$$m_f'' = \frac{m_{f\infty}''}{1 + \left(\frac{k}{t}\right)^n} \tag{1}$$

where $m_{f\infty}''$ is the asymptotic fouling density introduced previously, n is the Hill exponent, and k is a time constant. The model is versatile in being able to represent both sigmoidal and power-law trends in data depending on the exponent, n.

The originality of this work is in using the Hill-Langmuir relationship for the first time in predicting foulant binding and growth on wetting and nonwetting surfaces. The model also bears clear physical significance of the parameters. The parameter n, mathematically, is a measure of ultrasensitivity of the relationship to time and, physically, is a measure of cooperativity in biochemistry. In this work, the cooperativity concept is related to the change in the affinity of the surface for fouling as the nucleation and binding progresses such that, $n > 1$ denotes positive cooperation, $n < 1$ signifies a negative cooperation, and $n = 1$ is interpreted as a completely independent binding. The parameter k is the characteristic time for the half of the asymptotic maximum fouling mass, $m_{f\infty}''$, to deposit on the surface, and is physically significant in its importance in guiding system cleaning and maintenance.

As mentioned earlier, the asymptotic fouling density, $m''_{f\infty}$, represents an equilibrium between the effects of binding of the minerals on to the surface, measured in terms of a foulant material hardness, and the shear stress that tends to remove the deposits, and may be expressed as[45]:

$$m''_{f\infty} = \frac{K_D C_b p \psi}{\tau_a} \tag{2}$$

where K_D is particle deposition coefficient (m/s), C_b is bulk ion concentration (kg/m^3), p is the sticking probability and a dimensionless parameter, ψ, is scaling bond strength (N.s/m^2), and τ_a is shear stress (N/m^2) at the rotating drum surface. The particle deposition coefficient, K_D, is assumed to be equal to the mass transfer coefficient K_m that is related to the Schmidt number of the scaling solution through the Chilton-Colburn analogy[52]. This assumption holds for typical thermal engineering systems where the particle deposition is controlled by Brownian motion[53,54]. The bulk ion concentration, C_b, is constant for fixed temperature and is set to the corresponding saturation level: 7 kg/m^3 for 23 ℃ and 5 kg/m^3 for 50 ℃. Surface properties, such as the nonwetting properties and surface energies, are reflected in the scaling bond strength of ψ, whereas the effect of the rotation rate reflects itself in the shear stress τ_a. Moreover, the surface properties affect the nucleation reaction activation energy, E, that with temperature, T, both affect the sticking probability as given by the empirical relationship of Watkinson and Epstein[55], $p = \frac{C'}{u^2}\exp\left(-\frac{E}{RT}\right)$, in which C' is constant, R is universal gas constant, and u is the flow velocity. Note that the probability of binding increases with temperature and decreases with increased flow velocity. The activation energy is higher for nonwetting surfaces having low surface energy[19], which reduces the probability of fouling deposition.

Equation (2) suggests that the asymptotic fouling density increases with parameters that improve adhesion and binding of foulants on the surface namely, surface wettability and

temperature and decreases with increasing shear due to flow. Table 1 presents the values of $m''_{f\infty}$, k and n obtained from a least-squares regression fit of the Hill-Langmuir model, Equation (1), to the asymptotic fouling density measured in full suite of experiments covering the different surface type, fabrication route, temperature and rotational speed. The following physical trends are elucidated by the parameter values in Table 1:

1. The *asymptotic fouling density,* $m''_{f\infty}$, uniformly decreases with increasing rotation rate for all the surfaces, owing to the increased shear stress, τ_a, on the surface and is consistent with Equation (2), where the shear stress in the denominator has an inverse relationship with asymptotic fouling mass gain on the surface.

   Further, $m''_{f\infty}$ is lower for the nonwetting surfaces compared to the bare surface, reflecting the decrease in fouling bonding strength ψ which corresponds to decrease in surface energy of the nonwetting surfaces.

   Table 1 shows that the initial reduction in $m''_{f\infty}$ with rotational rate (from 100 rpm to 200 rpm) for the nonwetting surfaces is more dramatic compared to the bare copper surface, which is attributed to the lower adhesion strength of crystalized scale to the nonwetting surfaces. The almost zero slope between 200 rpm and 400 rpm for the nonwetting surfaces confirms that their anti-scaling effect is due to the lower surface energy rather than just the higher shear stress at the higher flow rate.

   The increase in $m''_{f\infty}$ with temperature in Table 1 is consistent with the increase in the sticking probability, p, through its Arrhenius relationship with temperature.

2. The *parameter* k denotes the time for half population of possible nucleation sites, which increase with increase in rotation rate. An increase in rotation rate leads to a higher shear stress that, in turn, increases the removal rate and leads to a delayed foulant accumulation. Moreover,

the value of k increases with increasing temperature, which reflects the fact that the asymptotic fouling density is higher at the higher temperatures, correspondingly necessitating a longer duration to achieve half the asymptotic value.

3. The *parameter* n is about unity for bare copper at both room and higher temperature. The value of $n = 1$ corresponds to independent cooperativity which means that the affinity of the bare copper surface to fouling binding does not change with time. This is expected as the bare surface already carries surface defects suitable for nucleation and crystal growth. On the other hand, the SHS with low surface energy has a high activation energy and hence lower nucleation rate compared to the bare case. As the first nuclei grow on the SHS the roughness and the local surface energies increase, which then increases the affinity of the surface for further fouling binding. This physical significance is clearly observed in the $n > 1$ values recorded for SHS in Table 1. The etched SHS has a higher affinity parameter than electrodeposited SHS, and furthermore, the affinity is greater at the higher temperature. The cooperativity coefficient n was recorded equal to 1 for LIS. Although LIS has low surface energy similar to SHS the dynamic nature of the infused lubricant causes wetting and cloaking of the deposited fouling, as imaged in Figure 6(c) and (f), which prevents change in the affinity of the LIS for fouling binding with time.

With the foregoing physical insights, the accuracy of the Hill-Langmuir model is investigated in Figure 7, which compares the fouling mass density predicted by the model (abscissa) with that obtained from the experimental measurements (ordinate) for all surfaces, fabrication methods, time, temperature and rotational speed studied, for a total of 60 points including the three rotation rates of 100 rpm, 200 rpm, and 400 rpm at 23 °C and 200 rpm at 50 °C, all for three times of 48 h,

96 h, 192 h. The different conditions of the experiments are denoted by the various markers as indicated in the plot. For the sake of clarity, experimental error bars around the mean values presented are omitted. The solid line diagonal to the plot frame denotes the line of exact agreement, while the dashed and the dash-dotted lines, respectively, represent the 10% and 20% error bars around the exact agreement.

Overall, the Hill-Langmuir model with the associated parameters presented in Table 1 is seen to be effective in predicting the time-evolution of fouling over time: ~85% of all data lies within the 20% error bands, with most of the points lying outside the 20% error being very low fouling mass values below about 0.75 $mg.cm^{-2}$. These data points correspond to either initial times or large rotation speed for which the fouling density values represent negligible fouling to be of any practical interest. In this region, the model predictions for some of the data points appear to be unchanged in the plot due to the differences being small to be discerned on the scale of the plot. Nevertheless, it is important to note that the model predictions compare well to experimental data within the error bars of the experiment. Furthermore, the model predictions lie evenly distributed on either side of the line of exact agreement, which suggests that the model does not have any systematic bias.

Considering the experimental measurement error bars, the proposed model has an accuracy of over 95% of data falling within the 20% error band. In comparison, the logistic regression model[47], when applied to the present data, was only 60% accurate with an 80% confidence interval[48]. Given that crystallization is inherently a stochastic process in its nature, the model is exceptionally accurate in predicting the fouling on smooth as well as nonwetting surfaces fabricated by the two different approaches, all in a unified way.

It is seen throughout the results presented in this article that nonwetting surfaces fabricated by either method demonstrate considerably reduced fouling compared to bare copper surface in a wide range of dynamic conditions. The effectiveness of the presented method for fabrication of nonwetting surfaces on copper may be extended to other materials such as brass and aluminum. The scaling mitigation on these surfaces are also of much practical significance and will be explored in a future work. Moreover, dynamic fouling investigations over a wider range of temperature may be pursued. Future studies may also focus on the process of fouling at early times with higher fidelity in the measurements.

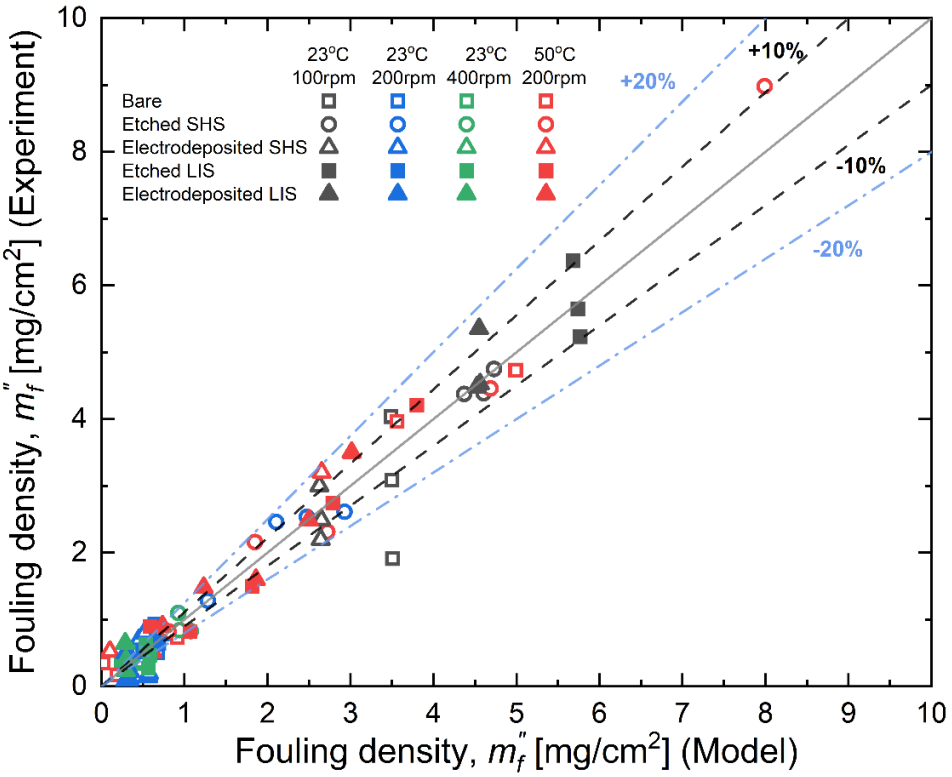

Figure 7: Comparison of the predictions of the Hill-Langmuir model with experimental measurements of fouling density for all the surfaces, rotational rate, and temperature studied, after 48 h, 92 h, and 192 h of immersion in calcium sulfate hemihydrate supersaturated solution.

4. CONCLUSIONS

The study presented the first systematic analysis of temperature-dependent dynamic fouling of calcium sulfate hemihydrate on superhydrophobic and lubricant-infused surfaces *vis-à-vis* bare surfaces using a Taylor-Couette flow setup. The effect of fabrication method on the performance of the resulting SHS and LIS was also assessed. Through systematic experiments, the time evolution of fouling mass per unit surface area was developed for a range of rotational speed and temperature. The study led to the following salient findings:

1. While bare copper exhibited a linear decrease in asymptotic fouling density with increasing *rotational speed*, the nonwetting surfaces exhibited a sharp initial decrease in fouling density followed by a relatively stable low fouling at the higher speeds.
2. Fouling increased with *temperature* due to the increase in the available energy in the system to overcome activation energy barrier and resulting increase in the fouling rate. However, SHS and LIS showed considerably reduced fouling compared to bare copper even at the high temperature at all times and in the asymptotic fouling density.
3. *Surface type (SHS/LIS)* had a meaningful effect on reducing deposited fouling compared to the unmodified bare copper surface. The superhydrophobicity of SHS and slipperiness of LIS showed superior resistance compared to the bare copper control sample. Electrodeposited SHS and LIS showed less scaling mass deposited at early times compared to their etched counterparts. With respect to the asymptotic fouling density, based on the mean values, electrodeposited SHS and LIS exhibited better anti-scaling characteristic. However, when considering the error bars in the fouling data, there was no distinct

difference between the two fabrication methods. It was shown that the asymptotic fouling was lower on all SHS and LIS by about 75% compared to bare copper surface.

4. A *Hill-Langmuir model* was developed based on the experimental studies for the first time for predicting foulant mass and its binding to both unmodified and modified nonwetting surfaces. The model was shown to capture the physics of the process and to be accurate in the predictions of the fouling mass density *vis-à-vis* the experimental measurements.

The study provides, for the first time, valuable insights into dynamic fouling process by juxtaposing different fabrication methods, different surface modifications, and various experimental environments.

ACKNOWLEDGMENT AND DISCLAIMER

The material reported in this publication is based upon work supported by the U.S. Department of Energy under Award Number DE-FE0031556. This publication was prepared as an account of work sponsored by an agency of the United States Government. Neither the United States Government nor any agency thereof, nor any of their employees, makes any warranty, express or implied, or assumes any legal liability or responsibility for the accuracy, completeness, or usefulness of any information, apparatus, product, or process disclosed, or represents that its use would not infringe privately owned rights. Reference herein to any specific commercial product, process, or service by trade name, trademark, manufacturer, or otherwise does not necessarily constitute or imply its endorsement, recommendation, or favoring by the United States Government or any agency thereof. The views and opinions of authors expressed herein do not necessarily state or reflect those of the United States Government or any agency thereof.

REFERENCES

[1] J. Zhao, M. Wang, H.M.S. Lababidi, H. Al-Adwani, K.K. Gleason, A review of heterogeneous nucleation of calcium carbonate and control strategies for scale formation in multi-stage flash (MSF) desalination plants, Desalination. 442 (2018) 75–88. https://doi.org/10.1016/J.DESAL.2018.05.008.

[2] J. Song, M. Liu, X. Sun, Model analysis and experimental study on scaling and corrosion tendencies of aerated geothermal water, Geothermics. 85 (2020) 101766. https://doi.org/10.1016/J.GEOTHERMICS.2019.101766.

[3] P.S. Goh, W.J. Lau, M.H.D. Othman, A.F. Ismail, Membrane fouling in desalination and its mitigation strategies, Desalination. 425 (2018) 130–155. https://doi.org/10.1016/J.DESAL.2017.10.018.

[4] F.L. Wang, Y.L. He, S.Z. Tang, Z.X. Tong, Parameter study on the fouling characteristics of the H-type finned tube heat exchangers, Int. J. Heat Mass Transf. 112 (2017) 367–378. https://doi.org/10.1016/J.IJHEATMASSTRANSFER.2017.04.107.

[5] M. Kamalipour, S.A.M. Dehghani, A. Naseri, S. Abbasi, Role of agitation and temperature on calcium sulfate crystallization in water injection process, J. Pet. Sci. Eng. 151 (2017) 362–372. https://doi.org/10.1016/J.PETROL.2016.12.039.

[6] T.H. Chong, R. Sheikholeslami, Thermodynamics and kinetics for mixed calcium carbonate and calcium sulfate precipitation, Chem. Eng. Sci. 56 (2001) 5391–5400. https://doi.org/10.1016/S0009-2509(01)00237-8.

[7] J.G. Lee, Y. Jang, L. Fortunato, S. Jeong, S. Lee, T.O. Leiknes, N. Ghaffour, An advanced online monitoring approach to study the scaling behavior in direct contact membrane distillation, J. Memb. Sci. 546 (2018) 50–60.

https://doi.org/10.1016/J.MEMSCI.2017.10.009.

[8] S. Tang, Y. Ji, K. Ge, Crystallization Kinetics and Mechanisms of Calcium Sulfate Dihydrate: Experimental Investigation and Theoretical Analysis, Ind. Eng. Chem. Res. 59 (2020) 21676–21684. https://doi.org/10.1021/ACS.IECR.0C04220.

[9] K.S. Song, J. Lim, S. Yun, D. Kim, Y. Kim, Composite fouling characteristics of CaCO3 and CaSO4 in plate heat exchangers at various operating and geometric conditions, Int. J. Heat Mass Transf. 136 (2019) 555–562. https://doi.org/10.1016/J.IJHEATMASSTRANSFER.2019.03.032.

[10] F. Alimi, A. Gadri, Kinetics and morphology of formed gypsum, Desalination. 166 (2004) 427–434. https://doi.org/10.1016/J.DESAL.2004.06.097.

[11] M. Crabtree, D. Eslinger, P. Fletcher, M. Miller, Fighting scale: removal and prevention, Oilfield. (1999).

[12] J.G. Tanquero, E.-S.A. Abdel-Aal, R.S. Farinato, H. El-Shall, B.M. Moudgil, Inhibition of calcium sulphate hemihydrate crystallization under simulated conditions of phosphoric acid evaporation, Can. J. Chem. Eng. (2021). https://doi.org/10.1002/CJCE.24210.

[13] D. Hasson, H. Shemer, A. Sher, State of the Art of Friendly "Green" Scale Control Inhibitors: A Review Article, Ind. Eng. Chem. Res. 50 (2011) 7601–7607. https://doi.org/10.1021/IE200370V.

[14] H. Zettler, M. Wei, Q. Zhao, H.U. Zettler, Influence of surface properties and characteristics on fouling in plate heat exchangers, Heat Transf. Eng. 26 (2007) 3–17. https://doi.org/10.1080/01457630590897024.

[15] M. Forster, M. Bohnet, Modification of molecular interactions at the interface crystal/heat transfer surface to minimize heat exchanger fouling, Int. J. Therm. Sci. 39 (2000) 697–708.

https://doi.org/10.1016/S1290-0729(00)00229-5.

[16] S.B. Subramanyam, G. Azimi, K.K. Varanasi, Designing Lubricant-Impregnated Textured Surfaces to Resist Scale Formation, Adv. Mater. Interfaces. 1 (2014) 1300068. https://doi.org/10.1002/ADMI.201300068.

[17] A. Baldelli, B. Bschaden, A. Amirfazli, D. Sameoto, Reproducibility of superhydrophobic and oleophobic polymeric micro surface topographies, Surf. Topogr. Metrol. Prop. 8 (2020) 045010. https://doi.org/10.1088/2051-672X/AB797E.

[18] A. Baldelli, J. Ou, D. Barona, W. Li, A. Amirfazli, Sprayable, Superhydrophobic, Electrically, and Thermally Conductive Coating, Adv. Mater. Interfaces. 8 (2021) 1902110. https://doi.org/10.1002/ADMI.201902110.

[19] G. Azimi, Y. Cui, A. Sabanska, K.K. Varanasi, Scale-resistant surfaces: Fundamental studies of the effect of surface energy on reducing scale formation, Appl. Surf. Sci. 313 (2014) 591–599. https://doi.org/10.1016/J.APSUSC.2014.06.028.

[20] D.E. Packham, Surface energy, surface topography and adhesion, Int. J. Adhes. Adhes. 23 (2003) 437–448. https://doi.org/10.1016/S0143-7496(03)00068-X.

[21] S. Keysar, R. Semiat, D. Hasson, J. Yahalom, Effect of Surface Roughness on the Morphology of Calcite Crystallizing on Mild Steel, J. Colloid Interface Sci. 162 (1994) 311–319. https://doi.org/10.1006/JCIS.1994.1044.

[22] H. Müller-Steinhagen, Q. Zhao, A. Helali-Zadeh, X.-G. Ren, The effect of surface properties on CaSO4 scale formation during convective heat transfer and subcooled flow boiling, Can. J. Chem. Eng. 78 (2000) 12–20. https://doi.org/10.1002/CJCE.5450780105.

[23] W.C. Cheong, P.H. Gaskell, A. Neville, Substrate effect on surface adhesion/crystallisation of calcium carbonate, J. Cryst. Growth. 363 (2013) 7–21.

https://doi.org/10.1016/J.JCRYSGRO.2012.09.025.

[24] A. Herz, M.R. Malayeri, H. Müller-Steinhagen, Fouling of roughened stainless steel surfaces during convective heat transfer to aqueous solutions, Energy Convers. Manag. 49 (2008) 3381–3386. https://doi.org/10.1016/J.ENCONMAN.2007.09.034.

[25] T. Zhang, Y. Wang, F. Zhang, X. Chen, G. Hu, J. Meng, S. Wang, Bio-inspired superhydrophilic coatings with high anti-adhesion against mineral scales, NPG Asia Mater. 2018 103. 10 (2018) e471–e471. https://doi.org/10.1038/am.2017.224.

[26] F. Signorelli, M.F.B. Sousa, C.A. Bertran, Interfacial Phenomena on the Inorganic Scaling Prevention, (2019). https://doi.org/10.1021/acsomega.8b02878.

[27] W. Jiang, J. He, F. Xiao, S. Yuan, H. Lu, B. Liang, Preparation and Antiscaling Application of Superhydrophobic Anodized CuO Nanowire Surfaces, Ind. Eng. Chem. Res. 54 (2015) 6874–6883. https://doi.org/10.1021/ACS.IECR.5B00444.

[28] H. Qian, Y. Zhu, H. Wang, H. Song, C. Wang, Z. Liu, H. Li, Preparation and Antiscaling Performance of Superhydrophobic Poly(phenylene sulfide)/Polytetrafluoroethylene Composite Coating, (2017). https://doi.org/10.1021/acs.iecr.7b03975.

[29] T.V.J. Charpentier, A. Neville, S. Baudin, M.J. Smith, M. Euvrard, A. Bell, C. Wang, R. Barker, Liquid infused porous surfaces for mineral fouling mitigation, J. Colloid Interface Sci. 444 (2015) 81–86. https://doi.org/10.1016/J.JCIS.2014.12.043.

[30] M.F.B. Sousa, G.F. Barbosa, F. Signorelli, C.A. Bertran, Anti-scaling properties of a SLIPS material prepared by silicon oil infusion in porous polyaniline obtained by electropolymerization, Surf. Coatings Technol. 325 (2017) 58–64. https://doi.org/10.1016/J.SURFCOAT.2017.06.038.

[31] S.M.A. Mousavi, R. Pitchumani, A Study of Corrosion on Electrodeposited

Superhydrophobic Copper Surfaces, Corros. Sci. 186 (2021) 109420. https://doi.org/10.1016/j.corsci.2021.109420.

[32] S.M.A. Mousavi, R. Pitchumani, Bioinspired nonwetting surfaces for corrosion inhibition over a range of temperature and corrosivity, J. Colloid Interface Sci. 607 (2022) 323–333. https://doi.org/10.1016/J.JCIS.2021.08.064.

[33] I.S. Bayer, Superhydrophobic Coatings from Ecofriendly Materials and Processes: A Review, Adv. Mater. Interfaces. 7 (2020) 2000095. https://doi.org/10.1002/ADMI.202000095.

[34] Y. Wang, X. Zhou, M. Yin, J. Pu, N. Yuan, J. Ding, Superhydrophobic and Self-Healing Mg-Al Layered Double Hydroxide/Silane Composite Coatings on the Mg Alloy Surface with a Long-Term Anti-corrosion Lifetime, Langmuir. 37 (2021) 8129–8138. https://doi.org/10.1021/ACS.LANGMUIR.1C00678.

[35] M. Tenjimbayashi, R. Togasawa, K. Manabe, T. Matsubayashi, T. Moriya, M. Komine, S. Shiratori, Liquid-Infused Smooth Coating with Transparency, Super-Durability, and Extraordinary Hydrophobicity, Adv. Funct. Mater. 26 (2016) 6693–6702. https://doi.org/10.1002/ADFM.201602546.

[36] VIII. Stability of a viscous liquid contained between two rotating cylinders, Philos. Trans. R. Soc. London. Ser. A, Contain. Pap. a Math. or Phys. Character. 223 (1923) 289–343. https://doi.org/10.1098/RSTA.1923.0008.

[37] A. Masoudi, P. Irajizad, N. Farokhnia, V. Kashyap, H. Ghasemi, Antiscaling Magnetic Slippery Surfaces, ACS Appl. Mater. Interfaces. 9 (2017) 21025–21033. https://doi.org/10.1021/ACSAMI.7B05564.

[38] T.A. Hoang, H.M. Ang, A.L. Rohl, Effects of temperature on the scaling of calcium sulphate

in pipes, Powder Technol. 179 (2007) 31–37. https://doi.org/10.1016/J.POWTEC.2006.11.013.

[39] W.L. Marshall, R. Slusher, Thermodynamics of Calcium Sulfate Dihydrate in Aqueous Sodium Chloride Solutions, 0-110°1,2, J. Phys. Chem. 70 (2002) 4015–4027. https://doi.org/10.1021/J100884A044.

[40] D.J. Preston, Y. Song, Z. Lu, D.S. Antao, E.N. Wang, Design of Lubricant Infused Surfaces, ACS Appl. Mater. Interfaces. 9 (2017) 42383–42392. https://doi.org/10.1021/acsami.7b14311.

[41] A. Haghdoost, R. Pitchumani, Fabricating Superhydrophobic Surfaces via a Two-Step Electrodeposition Technique, (2013). https://doi.org/10.1021/la403509d.

[42] J. Mullin, Crystallization, 2001. https://books.google.com/books?hl=en&lr=&id=Et0EtojQmvsC&oi=fnd&pg=PP1&dq=Mullin,+John+William&ots=Vt8B4VSzvO&sig=kWyzHA5Ys0-EwMvbDe7aA6_zVn8 (accessed July 20, 2021).

[43] C. Yoder, Ionic compounds: applications of chemistry to mineralogy, 2006. https://books.google.com/books?hl=en&lr=&id=JsiDDwAAQBAJ&oi=fnd&pg=PA1&dq=Yoder,+Claude+H.+Ionic+compounds:+applications+of+chemistry+to+mineralogy.+John+Wiley+%26+Sons,+2006.,+ref&ots=a5R416AGCh&sig=vdBtz-QNL9KSd9ulCNIVnJ81fpg (accessed July 20, 2021).

[44] A.R. Konak, A new model for surface reaction-controlled growth of crystals from solution, Chem. Eng. Sci. 29 (1974) 1537–1543. https://doi.org/10.1016/0009-2509(74)87004-1.

[45] D.Q. Kern, R.E. Seaton, A theoretical analysis of thermal surface fouling, 4 (1959) 258–262.

[46] R.L. Webb, W. Li, Fouling in enhanced tubes using cooling tower water: Part I: long-term fouling data, Int. J. Heat Mass Transf. 43 (2000) 3567–3578. https://doi.org/10.1016/S0017-9310(99)00395-6.

[47] P.F. Verhulst, Notice sur la loi que la population suit dans son accroissement, Corresp. Mathématique Phys. 10: (1838) 113–126. https://ci.nii.ac.jp/naid/10015246307 (accessed July 20, 2021).

[48] E. Nebot, J.F. Casanueva, T. Casanueva, D. Sales, Model for fouling deposition on power plant steam condensers cooled with seawater: Effect of water velocity and tube material, Int. J. Heat Mass Transf. 50 (2007) 3351–3358. https://doi.org/10.1016/J.IJHEATMASSTRANSFER.2007.01.022.

[49] A. Hill, The possible effects of the aggregation of the molecules of haemoglobin on its dissociation curves, J. Physiol. (1910).

[50] I. Langmuir, The adsorption of gases on plane surfaces of glass, mica and platinum, J. Am. Chem. Soc. 40 (1918) 1361–1403. https://doi.org/10.1021/JA02242A004.

[51] R. Gesztelyi, J. Zsuga, A. Kemeny-Beke, B. Varga, B. Juhasz, A. Tosaki, The Hill equation and the origin of quantitative pharmacology, Arch. Hist. Exact Sci. 2012 664. 66 (2012) 427–438. https://doi.org/10.1007/S00407-012-0098-5.

[52] R. Bird, W. Stewart, E. Lightfoot, Transport Phenomena revised 2nd Edition, (2006). https://highlandsranchhistoricalsociety.org/sites/default/files/webform/speaker_request_files/pdf-transport-phenomena-revised-2nd-edition-r-byron-bird-warren-e-stewart-edwin-n-lightfoot-pdf-download-free-book-73159db.pdf (accessed September 17, 2021).

[53] W. Li, Modeling liquid-side particulate fouling in internal helical-rib tubes, Chem. Eng. Sci. 62 (2007) 4204–4213. https://doi.org/10.1016/J.CES.2007.04.052.

[54] R. Gao, C. Shen, X. Wang, Y. Yao, Experimental study on the sticking probability and deposit bond strength of fouling in enhanced tubes, Int. Commun. Heat Mass Transf. 103 (2019) 17–23. https://doi.org/10.1016/J.ICHEATMASSTRANSFER.2019.02.010.

[55] H. Müller-Steinhagen, M.R. Malayeri, A.P. Watkinson, Heat exchanger fouling: Mitigation and cleaning strategies, Heat Transf. Eng. 32 (2011) 189–196. https://doi.org/10.1080/01457632.2010.503108.

Table 1. Parameters of the Hill-Langmuir model for calcium sulfate scaling on bare, SHS and LIS copper surfaces

Surface	$m''_{f\infty}$ [mg. cm^{-2}]				k [h]				n			
	23 ℃			50 ℃	23 ℃			50 ℃	23 ℃			50 ℃
	100 rpm	200 rpm	400 rpm	200 rpm	100 rpm	200 rpm	400 rpm	200 rpm	100 rpm	200 rpm	400 rpm	200 rpm
Bare copper	4.86	3.59	1.53	11.99	5.4	43.1	60.0	146.4	1.00	1.00	1.00	1.05
Etched SHS	3.51	0.68	0.30	5.32	1.0	3.6	16.0	75.2	1.32	1.35	1.30	2.90
Electrodeposited SHS	2.66	0.58	0.52	6.50	1.1	4.3	18.4	220.0	1.20	1.24	1.23	2.72
Etched LIS	5.80	0.71	0.60	5.98	1.0	5.1	5.3	110.0	1.00	1.00	1.00	1.00
Electrodeposited LIS	4.58	0.35	0.30	3.80	0.5	2.3	2.3	50.0	1.00	1.00	1.00	1.00